



Study of the electrochemical dissolution behavior of Nitinol shape memory alloy in different electrolytes for micro-ECM process

Abhijeet Sethi¹ · Biswesh Ranjan Acharya¹ · Partha Saha¹

Received: 13 November 2021 / Accepted: 14 July 2022 / Published online: 22 July 2022
© The Author(s), under exclusive licence to Springer-Verlag London Ltd., part of Springer Nature 2022

Abstract

Nickel-titanium alloy (Nitinol) is an excellent shape memory alloy (SMA) for microelectro-mechanical systems (MEMS) particularly in biomedical applications owing to its three excellent features shape memory effect (SME), superelasticity, and biocompatibility. The temperature-dependent material transformation properties of Nitinol SMAs make conventional machining difficult. Micro-ECM, a non-conventional machining process for conductive materials regardless of their strength and hardness, has the potential to fabricate microfeatures on Nitinol. This study presents the investigation on the electrochemical dissolution behavior of Nitinol in different electrolytes for micro-ECM. The influence of electrolytes on the nature of dissolution of Nitinol was studied by fabricating microchannels in three levels of parameters containing applied voltage and electrolyte concentration. The first three electrolytes were all aqueous neutral electrolytes, i.e., NaCl, NaNO₃, and NaBr. The aqueous NaNO₃ was successful in fabricating microchannels at all levels of process parameters. However, aqueous electrolytes form relatively a huge amount of sludge on the machined surface reducing both dissolution efficiency and machining accuracy. Thus, ethylene glycol-based NaNO₃ was used to fabricate microchannels with lower depth overcut (DOC), width overcut (WOC), and length overcut (LOC) with respect to aqueous NaNO₃ electrolyte. The potentiodynamic polarization (PDP) tests of Nitinol through cyclic voltammetry (CV) shows passive dissolution in aqueous electrolyte and active dissolution in non-aqueous electrolyte.

Keywords Micro-ECM · Nitinol · Microchannel · Sodium nitrate · Ethylene glycol · Polarization test

1 Introduction

Nickel-titanium alloy or NiTi belongs to a class of smart materials that show shape memory effect (SME) and pseudoelasticity and have the composition of Ni_xTi_{1-x}, where 0.47 ≤ x ≤ 0.51 [1]. It is popularly known as Nitinol, which is derived from the nickel titanium naval ordnance factory where it was discovered in the 1960s by Kauffman and Mayo [2]. The shape memory effect is the transition of a

material from a deformed state to an undeformed state when heated above its transition temperature. The transition is called martensitic transformation which happens due to the solid-state phase transformation where simple cubic austenitic crystal structure transforms to monoclinic martensite crystal structure [3]. Nitinol also exhibits pseudoelasticity otherwise named superelasticity where a large strain can be induced during mechanical loading [4]. NiTi forms a titanium-rich oxide layer on the surface, hence showing excellent biocompatibility [5]. The above three features, i.e., SME, superelasticity, and biocompatibility, makes NiTi the preferred SMA for MEMS particularly in biomedical applications [6]. These MEMS devices perform significant tasks in a scaled-down miniaturized volume. Sensing and analyzing light and mechanical signals, sequencing biomolecules, mixing, processing, and analyzing the ultra-little volume of chemicals are some of the regular activities realized by these miniaturized machines [7]. The MEMS has various advantages like quick response time (e.g., airbag

✉ Partha Saha
psaha@mech.iitkgp.ernet.in

Abhijeet Sethi
abhijeet.ab89@gmail.com

Biswesh Ranjan Acharya
bishweshacharya@gmail.com

¹ Department of Mechanical Engineering, Indian Institute of Technology Kharagpur, Kharagpur, West Bengal 721302, India

sensors), usage of fewer consumables (e.g., Lab-on-a-Chip), high resolution and efficiency (e.g., inkjet printer head, microchemical reactor), and portability [8]. The actuators form the fundamental system in the MEMS and SMAs are now extensively used as a material of choice for actuators. Nitinol MEMS devices such as microvalves, micropumps, microgrippers, actuated microendoscope, spaces, nerves clamp, and tactile displays are some of the examples that were reported over the last decade [9]. These devices often require the fabrication of microfeatures on Nitinol SMAs, and there are both traditional and non-traditional ways to manufacture these microscale features [10]. Traditional manufacturing processes such as turning [11], milling [12], and drilling [13] and non-traditional machining processes like laser processing [14], electrodischarge machining (EDM) [15], abrasive water jet machining (AWJM) [16], chemical etching [17], and electrochemical machining [18–20] were used in the past for Nitinol microfabrication.

Microelectrochemical machining (micro-ECM) is a promising method for microfeature fabrication due to advantages like defect-free surface generation, negligible tool wear, and the capability to machine any conductive material regardless of its strength and hardness [20]. Micro-ECM was used to manufacture microfeatures on some of the advanced materials like stainless steel [21], titanium and its alloys [22], nickel alloys [23], tungsten [24], and tungsten carbide [25]. Micro-ECM has various potential applications in a wide range of industrial sectors [20]. Micro-ECM can provide an alternative machining method for the fabrication of microfeatures on Nitinol surface by anodic dissolution. Takashi Mineta performed masked pulsed electrochemical etching of Nitinol with 1 mol l^{-1} LiCl–ethanol electrolyte to fabricate microgrooves on the surface. He had obtained etched microgrooves with 20- μm in-depth [26]. Ma et al. performed confined etchant layer technique to manufacture intricate 3D microfeatures on Nitinol with an etched pattern having micrometer accuracy. However, the microstructures obtained were having a depth of less than 1 μm [27]. Lee et al. used pulse ECM for the fabrication of microgrooves on NiTi SMA and studied the parametric influence on the rate of material dissolution and groove depth. They used an electrolyte that generated NaNO_2 and tartarate for anodic dissolution, where tartarate prevents the formation of $\text{Ni}(\text{OH})_2$ on the surface [19]. Maurer et al. used electrochemical micromachining (EMM) with pulsed DC power supply to machine microstructures of 3- μm depth on NiTi SMA using 1 M methanolic-LiCl [28]. Ao et al. fabricated microgrooves on NiTi SMA through EMM with non-aqueous ethylene glycol (EG)-based NaCl electrolyte with a concentration of 40 g/L and an applied voltage of 14 V with 10-kHz pulse frequency. They added ethanol in the range of 0–30 vol% to the solution to improve the surface quality of the microstructures and found the lowest Ra of 0.417 μm at 20 vol% of ethanol. Also, they obtained the lowest average

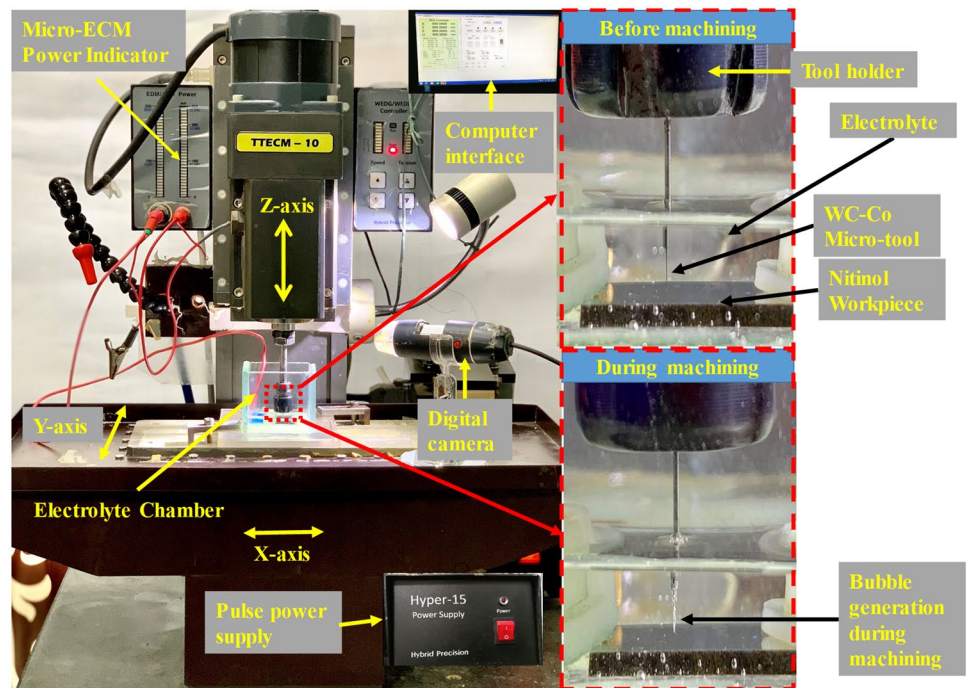
groove width of 249.3 μm at 10 vol% ethanol mixed EG-based NaCl electrolyte with the use of a 100- μm -diameter microtool. They concluded that the addition of ethanol to EG NaCl solution can reduce the formation of oxide films [29]. However, the surface roughness and the accuracy of the microchannel can further be improved. Mouliprasanth and Hariharan fabricated microholes in NiTi SMA using non-passivating electrolyte (NPE) of aqueous NaCl and passivating electrolyte (PE) of aqueous NaNO_3 through the micro-ECM process. They concluded that to get a better MRR, NPE electrolyte can be used, and for better surface integrity, PE electrolyte can be used [30].

The abovementioned investigations promoted the fabrication of microstructures on Nitinol SMA through chemical etching and micro-ECM where the process parameters, machining accuracy, and surface integrity were studied. The electrolytes that are used are ethanol-based lithium chloride (LiCl) which is costly and hydrofluoric acid (HF) with nitric acid (HNO_3) which is toxic in nature. Also, there were very limited attempts made that are aimed at exploring the dissolution behavior of Nitinol in aqueous neutral solutions which are commercially used in ECM. Thus, further research on the machining performance of the micro-ECM technique for Nitinol SMA in the aqueous neutral electrolyte is required. Therefore, in this paper, a thorough investigation was done to evaluate the performance of aqueous neutral electrolytes like sodium chloride (NaCl), sodium nitrate (NaNO_3), and sodium bromide (NaBr) to find out the effective dissolution of Nitinol in the microdomain by fabricating microchannels. Also, EG-based non-aqueous electrolyte was used to fabricate more accurate microchannels through the micro-ECM process. Moreover, to understand the electrochemical dissolution behavior of Nitinol in these electrolytes, potentiodynamic polarization tests were conducted.

2 Experimental setup

Experimentation for fabrication of microchannel by micro-ECM was conducted in TTECM-10 (table-top-type micro-ECM CNC machine tool) of Synergy Nanosystems, Mumbai. The machine consists of a computer, pulsed DC power supply, machining chamber, digital camera, and electrolyte circulation and filtration unit. Figure 1 shows the machine and its components. The machine has the provision of three CNC linear stages in the X, Y, and Z axes. The resolution for each stage is 0.1 $\mu\text{m}/\text{step}$, and the control of stepper motors is governed by a computer with the help of Hyper 2GUI software. The machine chamber is provided with horizontal X and Y motions, and the Z motion is given to the microtool holder perpendicular to the machining chamber along with the rotational motion. The machine has a power supply that can generate a maximum of 500-kHz frequency voltage pulses for microfabrication

Fig. 1 Microelectrochemical machine, TTECM-10



purposes. A digital camera is attached to the machine for online monitoring and measurement of microtools for successive experiments without removing them from the tool holder.

The potentiodynamic polarization experiments were conducted in an electrochemical cell having three electrodes with the help of Biologic SP 150 potentiostat as shown in

Fig. 2. The three electrodes used for the experiments are a reference electrode (saturated Ag/AgCl), an auxiliary electrode (platinum wire), and a working electrode (Nitinol sheet). Every one of the given potentials was determined against the standard hydrogen electrode (SHE). All the electrodes were connected with a PC-controlled potentiostat

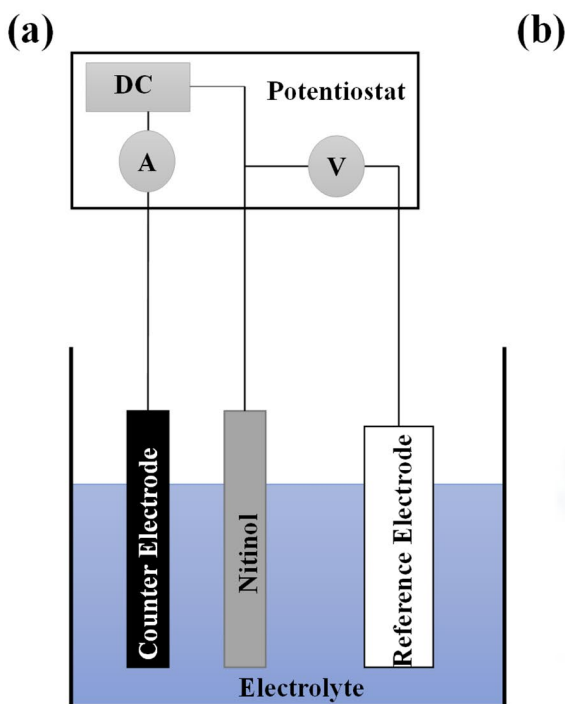
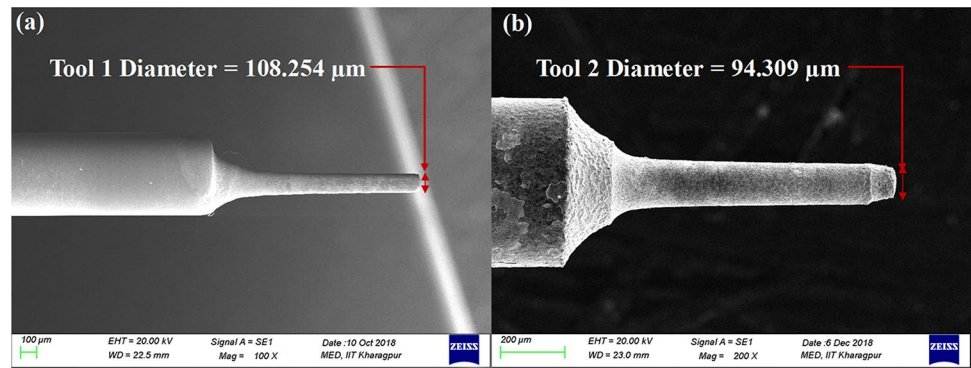


Fig. 2 a Schematic of the potentiodynamic polarization test experimental setup. b Biologic SP 150 potentiostat

Fig. 3 SEM images of in situ-fabricated microtool used for microchannel generation purpose



Biologic SP150. The exposed surface area of the working electrode Nitinol sheet was kept to 1 cm^2 .

3 Materials and methods

For the microtool fabrication process, cylindrical rod of tungsten carbide (WC–Co) having 500- μm diameter was used. The process is in situ as the TTECM-10 was used for the fabrication process by using the reverse polarity, and the same machine was used for the microchannel fabrication by straight polarity without removing the microtool. The diameter of the cylindrical WC rod is first reduced by electrodischarge grinding (EDG) with a brass block as cathode and a WC microrod as the anode. Then with the help of the wire electrochemical process (WECM), the surface of the fabricated microtool is improved by taking a 250- μm diameter of brass wire as cathode and the EDG fabricated

microtool as the anode [25]. There are two microtools with diameter 108.254 μm and 94.309 μm that have been used in the microchannel fabrication through the micro-ECM process. The images of the microtool obtained through a scanning electron microscope (SEM) are given in Fig. 3.

For this study, commercial Nitinol (52% Ni and 48% Ti) sheets of 1-mm thickness were used. For microchannel fabrication in micro-ECM, the samples were ultrasonically cleaned using acetone. For potentiodynamic polarization (PDP) analysis, the samples were prepared on a Buehler-Phoenix 4000 machine through grinding and polishing using SiC papers down to 2500 grit and diamond pastes (9, 3, then 1 μm) from Struers. After that, ultrasonic cleaner was used to clean the samples with acetone and deionized water. The prepared samples for microchannel fabrication through the micro-ECM process and PDP tests are shown in Fig. 4 along with their surface composition obtained from energy-dispersive spectroscopy (EDS) analysis.

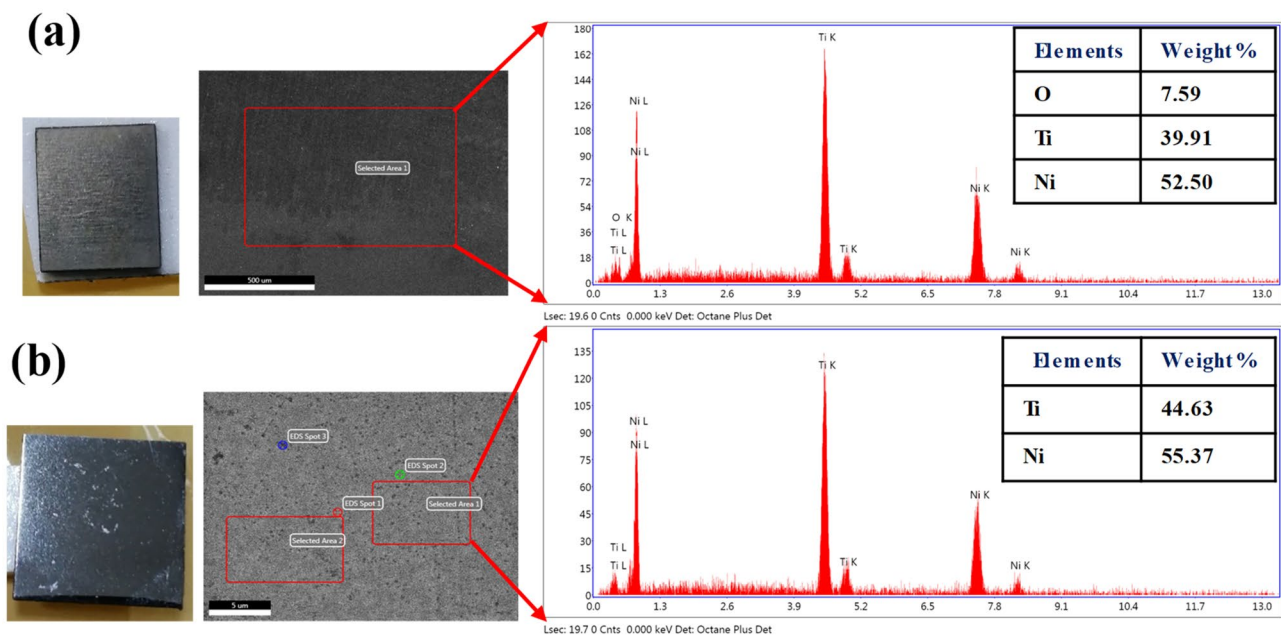


Fig. 4 **a** Sample for microchannel fabrication through micro-ECM with EDS analysis. **b** Sample for PDP tests with EDS analysis

Table 1 Electrolytes with their concentration for micro-ECM and PDP test

S. no.	Description	Molar concentration (M)	
		Micro-ECM	PDP test
1	Sodium chloride (NaCl)	0.1, 0.15, 0.2	0.1
2	Sodium nitrate (NaNO ₃)	0.1, 0.15, 0.2	0.1
3	Sodium bromide (NaBr)	0.1, 0.15, 0.2	0.1
4	Ethylene glycol and sodium nitrate (EG + NaNO ₃)	0.1, 0.15, 0.2	0.1

The electrolytes were used for the possibility of electrochemical dissolution of Nitinol by trying to generate microchannels, applying mask-less micro-ECM technique, that are aqueous neutral solutions of NaCl, NaNO₃, and NaBr. Also, ethylene-based NaNO₃ non-aqueous electrolytes were studied for their effect on the electrochemical dissolution of Nitinol. The electrolytes and their concentrations used for both the fabrication of microchannel as well as PDP tests are given in Table 1.

The layer-by-layer material removal by scanning method was employed to fabricate a microchannel of 2-mm length on the surface of a 1-mm-thick Nitinol sheet. The microchannels were fabricated with a downward feed (V_1) of 0.1 μm/s and a scanning feed (V_2) of 0.5 μm/s with 5-μm layer thickness. A total depth of 10 μm is given for microchannel fabrication with a 5-μm layer thickness. The schematic view of microtool movement during the generation of the microchannel is given in Fig. 5. The experiments were conducted in three levels of parameters with each level containing a combination of electrolyte concentration and applied voltage. The three levels of parameters are low levels containing 0.1 M concentration and 8 V applied voltage, mid-level with 0.15 M concentration and 12 V applied voltage, and high level of parameters with 0.2 M concentration and 16 V applied voltage whereas other parameters were

kept constant for each level. A range of trial experiments was conducted to find out the suitable input process parameters like electrolyte concentration, applied voltage, and tool feed rate. All the micro-ECM parameters that were used to fabricate the microchannels are given in Table 2.

After completion of the experiment, high-resolution images and the energy-dispersive spectroscopy (EDS) data of all the samples were taken through a scanning electron microscope (SEM). The machining of Nitinol through micro-ECM generates reaction products that are attached to the surface. These reaction products also called sludge containing oxides of either Ni or Ti or sometimes both. Thus, to understand the dissolution mechanism, SEM and EDS analysis of the samples with sludge were carried out. Then, all the samples were cleaned and SEM images were taken for surface integrity analysis. The average surface roughness of the machined sample was calculated at the midline along the length of the workpiece using a CCI non-contact-based surface profilometer to study the dissolution efficiency. The profile depth was obtained from the 3D profile which was generated through the profilometer.

Further, the effect of electrolytes on the accuracy of the fabricated microchannel was evaluated based on width overcut (WOC), depth overcut (DOC), and length overcut (LOC). The schematic showing width, depth, and length of a microchannel are given in Fig. 6. The WOC, DOC, and LOC are the excess material removed across the width, depth, and length of the microchannel, respectively, and are calculated according to the following formulas.

$$\text{Width overcut (WOC)} = \frac{\sum_i^n (w - d)}{2n}$$

$$\text{Depth overcut (DOC)} = H_2 - H_1$$

$$\text{Length overcut (LOC)} = L_2 - L_1$$

Fig. 5 Schematic view of microtool movement during generation of microchannel

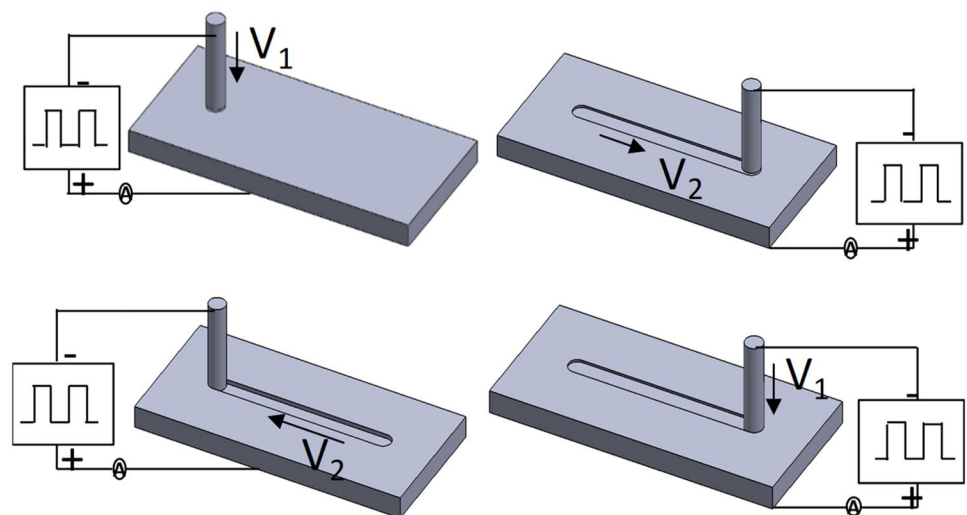


Table 2 Micro-ECM process parameter setup for microchannel generation on Nitinol

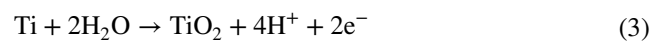
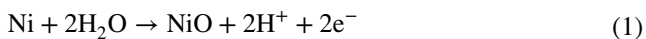
Sl no.	Process parameter	Nature	Low level	Mid level	High level
1	Electrolyte concentration	Variable	0.10 M	0.15 M	0.20 M
2	Applied voltage	Variable	8 V	12 V	16 V
3	Pulse frequency	Fixed		500 kHz	
4	Pulse on time	Fixed		1 μ s	
5	Pulse off time	Fixed		1 μ s	
6	Tool RPM	Fixed		500 rpm	
7	Downward feed (V_1)	Fixed		0.1 μ m/s	
8	Scanning feed (V_2)	Fixed		0.5 μ m/s	
9	Layer thickness	Fixed		5 μ m	
10	Total depth	Fixed		10 μ m	

where $i = 1, 2, \dots, n$ and “ n ” is the number of locations where channel width was measured, w = channel width, d = microtool diameter, H_1 = depth given to the micro tool during microchannel fabrication, H_2 = actual depth obtained, L_1 = length given to the micro tool during microchannel fabrication, and L_2 = actual length obtained.

4 Results and discussions

4.1 Effect of aqueous neutral electrolytes on anodic dissolution of Nitinol

One of the major problems related to the electrochemical dissolution of Nitinol is surface oxidation in atmospheric conditions. When exposed to a medium-containing oxygen, Nitinol forms a passive oxide film on its surface [29] which is also confirmed by the EDS analysis in Fig. 4a. According to the electrochemical Pourbaix diagram of Nitinol in aqueous solution, it forms oxide film which consists of TiO_2 and NiO as per the equations below [31].



Some studies suggest that the oxide film is dual in nature with TiO_2 on the top which is in contact with the NiO sublayer [31, 32]. However, resistance of this NiO sublayers to pitting is much lower, resulting in Ni dissolution through pores in the outermost TiO_2 film. In the case of aqueous NaCl solution, it can be seen that from the SEM images in Fig. 7 at all levels of parameters, a solid sludge layer is developed on the machined surface. The energy-dispersive spectroscopy (EDS) analysis of the sludge layer is given in Table 3 which shows the presence of titanium, nickel, and oxygen at all level parameters indicating the presence of oxides of both titanium and nickel. Also, with the increase in electrolyte concentration and applied voltage, the amount of oxygen increases and then decreases. Moreover, the amount of Ni content of the sludge decreases and

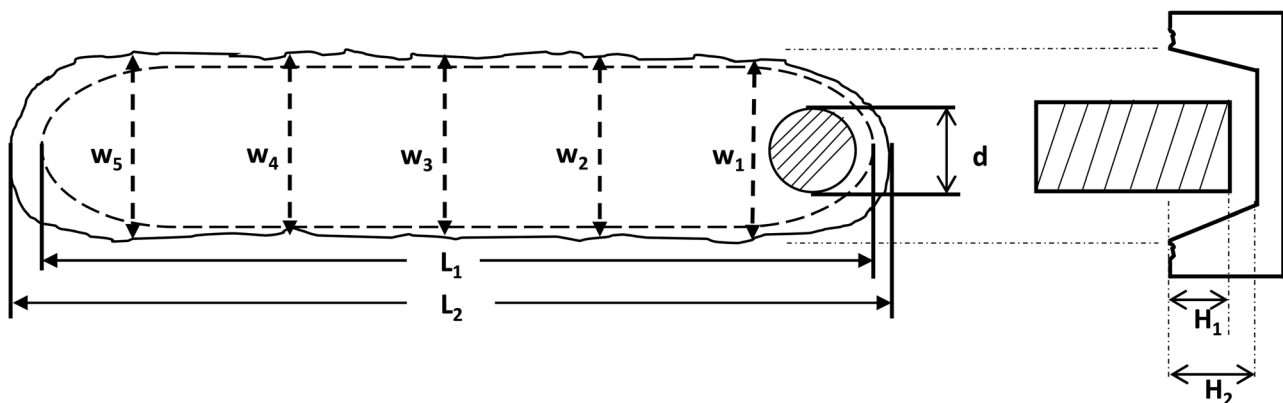
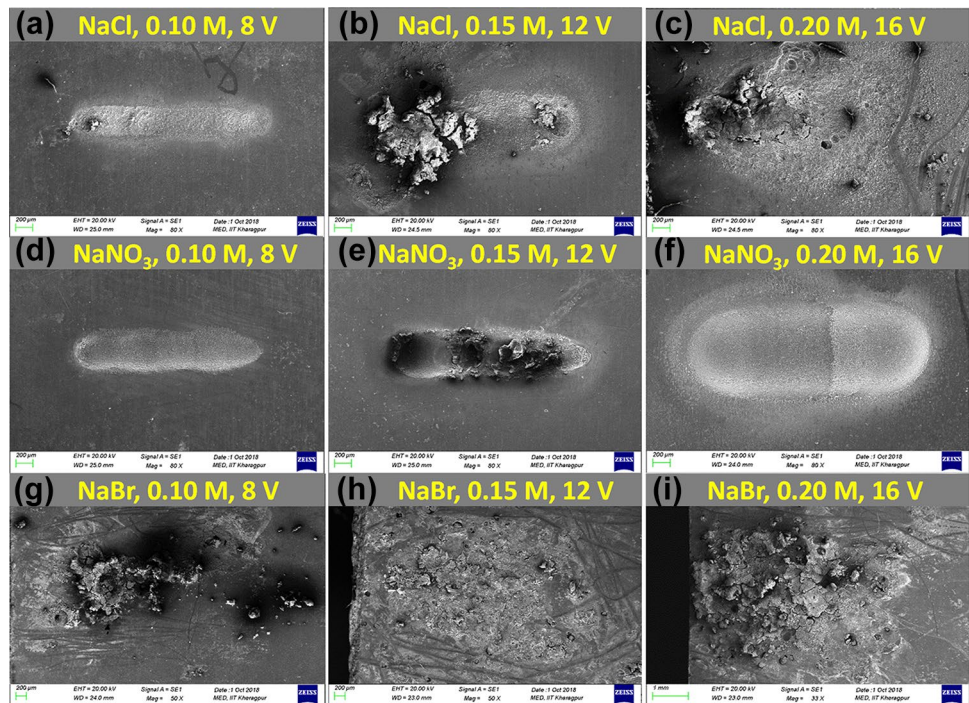
**Fig. 6** Schematic showing width, depth, and length of a microchannel

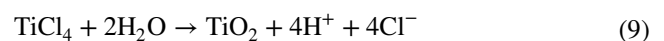
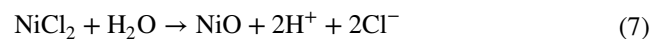
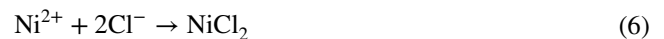
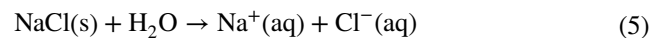
Fig. 7 Sludge growth on the specimen for different electrolyte conditions under three levels of parameters



then increases with the increases in the process parameters. The aggressive Cl^- ions in case of aqueous NaCl solution attack the oxide layer, causing NiO to dissolve from the surface. The decrease in Ni content of the sludge confirms the higher dissolution of NiO than TiO_2 . As the TiO_2 is dense and sticky in nature, it restricts the metal dissolution. The process of dissolution of Nitinol in an aqueous solution follows two processes. First is the adsorption of OH^- ions which leads to passivity, and then, the second process corresponds to the adsorption of anions (Cl^- , NO_3^- , Br^- , etc.). The adsorption of anions occurs most frequently in oxide defects such as minor cuts, dips, cracks, or pores, where the oxide layer is thin and the electric field is strong. The adsorption of anions on the oxide layer creates soluble

salts with cations from the oxide which creates nucleation of dissolutions otherwise called pits. Once these pits are created, they continue to activate local dissolution by the autocatalytic process. According to the reference [33], Ni^{2+} and Ti^{4+} ions from Eqs. (2) and (4) react with Cl^- from the solution to form NiCl_2 and TiCl_4 , respectively, which thereafter reacts with H_2O to form again NiO and TiO_2 as shown in the equations. NiCl_2 is easily soluble in water, and most of the NiCl_2 dissolves into the electrolyte. However, TiCl_4 is very sticky and attaches to the surface of the anode. Also, the formation of TiO_2 again on the anode has a strong binding force on the surface of the Nitinol workpiece. Thus, the formation of TiCl_4 and subsequent TiO_2 prevents the uniform dissolution of Nitinol in the aqueous NaCl solution.

In aq. NaCl solution:



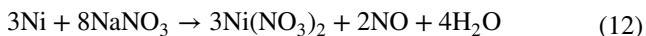
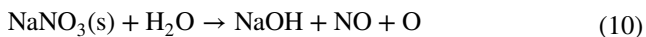
In the case of neutral electrolyte aqueous NaNO_3 , it could be observed from Fig. 7 that at the low level of parameters,

Table 3 EDS data of sludge growth on the specimen for different electrolyte conditions under three levels of parameters

Electrolyte	Parameters	Element weight (%)		
		Ti	Ni	O
NaCl	0.1 M, 8 V	36.37	32.78	30.84
	0.15 M, 12 V	26.55	17.52	55.92
	0.20 M, 16 V	31.67	25.40	42.94
NaNO_3	0.1 M, 8 V	38.15	40.91	20.00
	0.15 M, 12 V	23.43	27.15	42.92
	0.20 M, 16 V	36.69	36.98	26.33
NaBr	0.1 M, 8 V	34.84	20.19	44.97
	0.15 M, 12 V	21.99	34.57	43.44
	0.20 M, 16 V	26.07	35.12	38.81

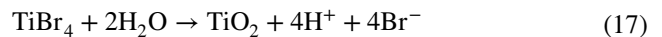
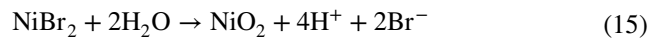
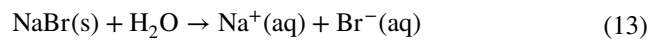
the volume of sludge attached to the surface is low. But at the mid-level parameters, there is visible sludge attached to the surface. However, at a high level, the amount of sludge again decreases. The EDS data of sludge in Table 3 shows that for all the levels of parameters, Ni, Ti, and O are present in the sludge. However, the amount of oxygen in the sludge is low in comparison to NaCl. Moreover, the amount of Ni and Ti content of the sludge remains almost equal suggesting a uniform dissolution of both NiO and TiO₂. At the mid-level parameters, the amount of oxide formation is high, and thus, it prevents a uniform dissolution. NaNO₃ is a known passivating electrolyte that is used to achieve better accuracy in the case of ECM-based micromachining. According to the Pourbaix diagram for the titanium-water system, the dissolution of TiO₂ happens in the alkaline range [34]. NaNO₃ reacts with water to form NaOH which increases the pH of the solution and TiO₂ reacts with NaOH to form a soluble complex Na₂TiO₃ [35]. Once the outermost TiO₂ gets dissolved, the lower Ni layer gets dissolved through the formation of Ni(NO₃)₂. The above dissolution mechanism enhances not only the uniform electrochemical reaction but also the localized dissolution.

In aq. NaNO₃ solution:



Further experiments were conducted with the aqueous electrolyte of NaBr. From Fig. 7, it can be seen that a large amount of sludge is generated on the surface of Nitinol for all the levels of parameters. The EDS analysis of sludge from Table 3 shows that a high percentage of oxygen is present due to the formation of titanium and nickel oxide during the machining process. At the low level of parameters, the quantity of Ti is more than Ni. However, for the mid- and high-level parameters, amount of Ni is more in the sludge compared to that of Ti. The oxide layer NiO and TiO₂ forms complexes like NiBr₂ and TiBr₄ in the aqueous NaBr solution [34, 36]. Thus, the dissolution of Nitinol in aqueous NaBr solution is governed by the solubility of these two complexes. Br⁻ ions have the strongest ability to penetrate TiO₂ leading to local dissolution otherwise called pitting. The clusters of TiBr₄ molecules serve as nuclei of pits, and these are generated on the sites with increased electronic conductivity of oxide film [34]. At the high level of parameters, the concentration of anodic product TiBr₄ is very high at the metal surface and would exceed the solubility product, thus precipitating the salt on the surface as a thick layer which subsequently hinders the dissolution.

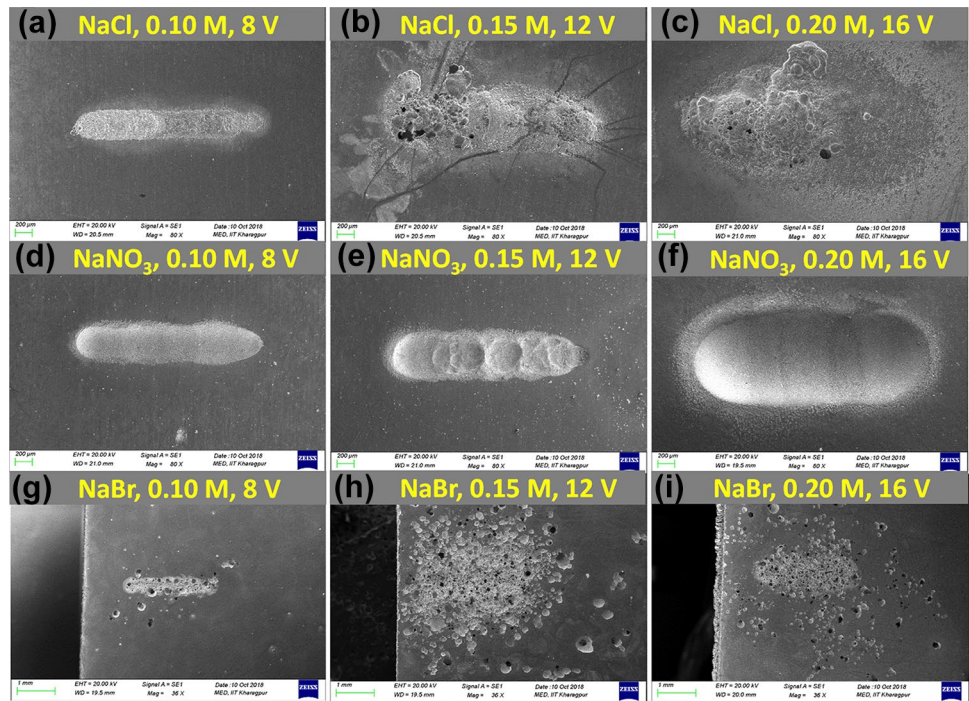
In aq. NaBr solution, the following reactions may take place:



After cleaning the workpiece, the SEM images were taken and are given in Fig. 8. Also, the high magnification SEM images of the surface of microchannels for all the parameters are given in Fig. 9. The average surface roughness (R_a) of the machined surface of the Nitinol was calculated at the midline along the length of the workpiece using a CCI non-contact 3D surface profilometer. Also, the depth of the microchannels was obtained at different regions from the 3D surface profile, and then, the average depth was considered. The accuracy parameters like average surface roughness (R_a), width overcut (WOC), depth overcut (DOC), and length overcut (LOC) were calculated and are given in Table 4. From Fig. 8, it can be seen that in the case of aqueous NaCl solution at low-level parameters, a channel is fabricated with WOC, DOC, and LOC at 113.72 μm, 36.78 μm, and 213.98 μm, respectively. However, in the case of mid-level and high-level parameters, the anodic dissolution of Nitinol is uncontrolled with an uneven and irregular surface, and thus, the channel formation was unsuccessful. If the high-resolution SEM images in Fig. 9 are referred, the surface shows highly non-uniform dissolutions, and with the increase in the level of parameters, the non-uniformity of the surface increases. To study the surface integrity, the relationship between average surface roughness (R_a) and the level of process parameters for different electrolytes is given in Fig. 10. The R_a is found to be 2.155 μm for aqueous NaCl electrolyte at the low level of parameters, increases up to 3.795 μm at mid-level parameters, and slightly decreases to 3.675 μm at high level. The higher R_a value in the case of aqueous NaCl electrolyte may be due to the formation of TiCl₄ on the surface which results in the variation of dissolution of Nitinol.

In the case of an aqueous NaNO₃ solution, a controlled dissolution can be seen at all levels of parameters (Fig. 8). The R_a values of 1.17 μm, 8.906 μm, and 0.846 μm are measured for low, mid, and high levels of parameters, respectively; thus, a uniform dissolution of Nitinol can be assumed. At the mid-level parameters, the R_a value is high due to the

Fig. 8 Machined specimen after cleaning for different electrolyte conditions under three levels of parameters



waviness nature of the surface. The 3D profile of the micro-channel fabricated in NaNO_3 electrolyte with 0.2 M and 16 V parameters is given in Fig. 11. In the case of NaNO_3 for the high level of the parameters, the lowest surface roughness of $0.848 \mu\text{m}$ was obtained confirming a better uniform dissolution of Nitinol in the NaNO_3 electrolyte. The high magnification SEM images, in the case of NaNO_3 , show a smoother surface in comparison to NaCl electrolyte. From

Table 4, it can be seen that the accuracy parameters like WOC, DOC, and LOC increase with the increase in the level of the parameters. As the dissolution rate increases with the increase in electrolyte concentration and applied voltage, the overcut increases.

However, in the case of aqueous NaBr at all levels of parameters, the channel fabrication was not successful. From Fig. 8, it can be observed that there is uncontrolled and

Fig. 9 Surface texture of micro-channel generated by micro-ECM under different electrolyte condition under three levels of parameters

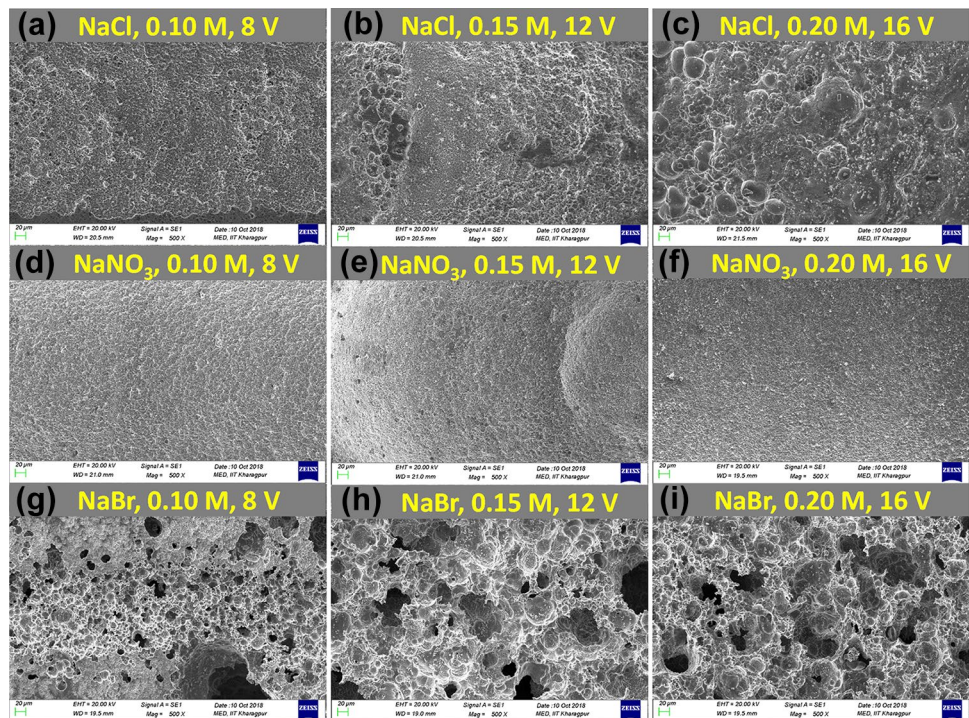
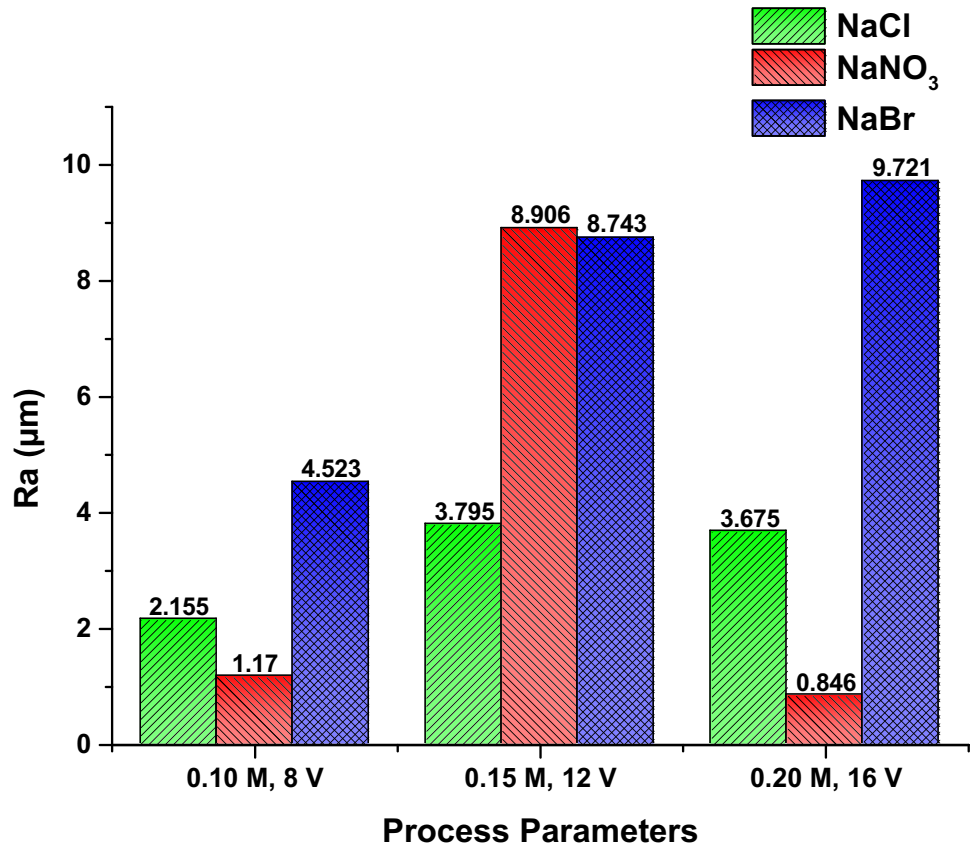


Table 4 Experimental outcomes of accuracy parameters

Expt. no	Process parameters		Electrolytes	R_a (μm)	WOC (μm)	DOC (μm)	LOC (μm)		
	Electrolyte concentration (M)	Applied voltage (v)							
1	0.10	8	NaCl	2.155	113.72	36.78	213.98		
2	0.15	12		3.795		164.44			
3	0.20	16		3.675		268.43			
4	0.10	8	NaNO ₃	1.17	153.95	110.95	189.86		
5	0.15	12		8.906		168.58		147.55	297.21
6	0.20	16		0.846		498.56		306.92	769.91
7	0.10	8	NaBr	4.523		20.17			
8	0.15	12		8.743		162.94			
9	0.20	16		9.721		145.86			
10	0.10	8	EG + NaNO ₃	0.891	143.77	56.33	376		
11	0.15	12		0.25		71.91		54.75	281.55
12	0.20	16		0.424		67.89		101.88	308.02

uneven dissolution, and large pitting areas were formed at all levels of parameters. The pitting area drastically increased in the mid-level parameters and then again reduces in the high-level parameters. The pits formed are having shallow depths as the DOCs are found to be 20.17 μm , 162.94 μm , and 145.86 μm , respectively, for the low, mid, and high

levels of parameters. The Br⁻ ions are aggressive halide anions which easily penetrate the weak points of the surface oxide layer to initiate localized corrosion creating pits. The high magnification SEM image of these pits in Fig. 9 shows facets and linked cavities with a porous structure that decreases surface roughness. The several pit formation

Fig. 10 Relationship between average surface roughness (R_a) and the level of process parameters for NaCl, NaNO₃, and NaBr electrolyte

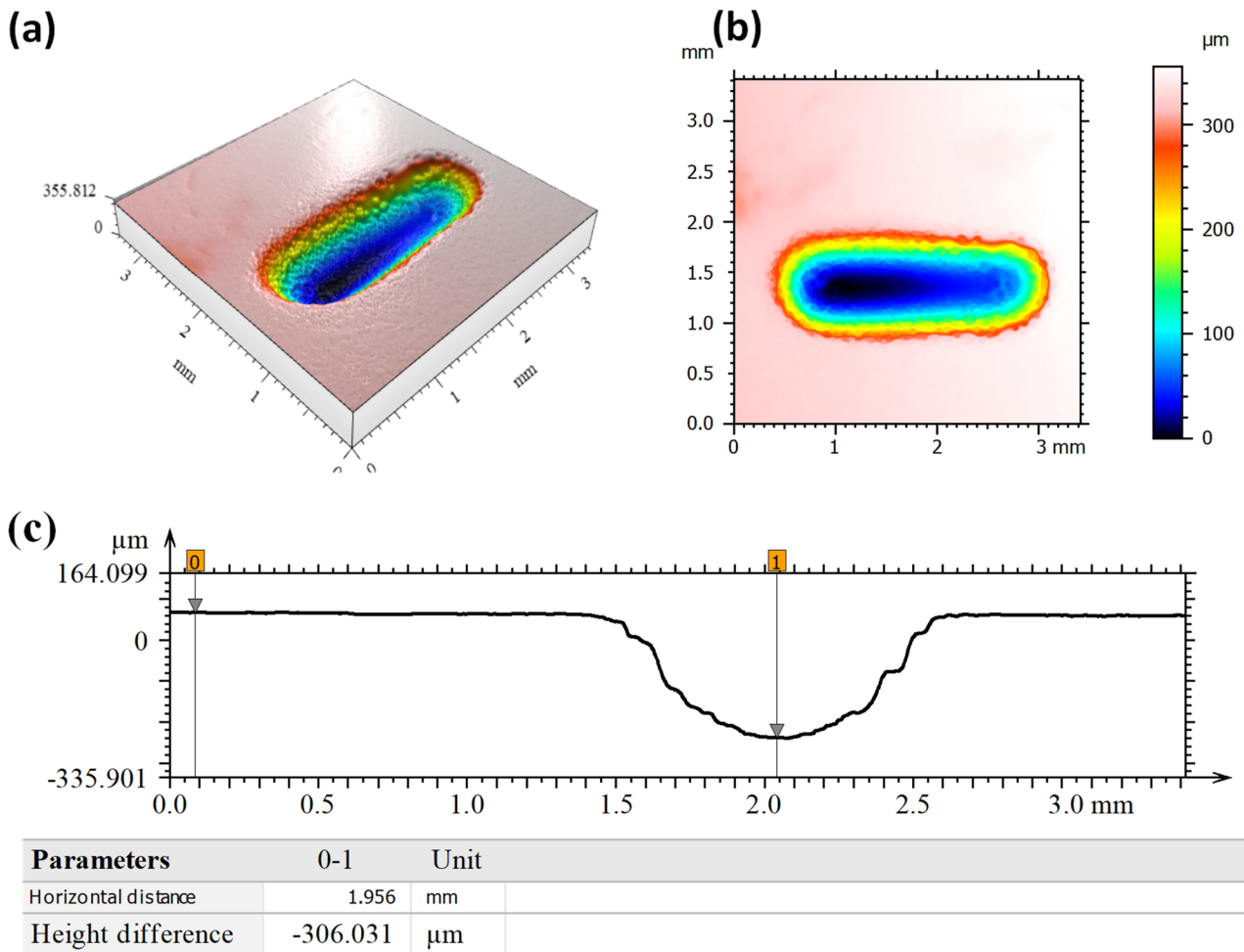


Fig. 11 The 3D surface profile obtained through Taylor Hobson CCI profilometer for the machined surface obtained in NaNO₃ electrolyte with 0.2 M and 16 V: **a** 3D profile, **b** 2D profile, and **c** depth measurement

without any localized dissolution for Nitinol in NaBr solution led to an irregular surface profile and subsequent failure in microchannel formation. The R_a values were measured at 4.523 μm, 8.743 μm, and 9.721 μm, respectively, for the low, mid, and high level of parameters indicating a non-uniform dissolution Nitinol in the case of NaBr solution. Figure 10 shows that the average surface roughness in the case of NaBr is on the higher side with respect to both NaCl and NaNO₃ electrolytes, and the best possible dissolution was obtained in the case of NaNO₃ electrolyte.

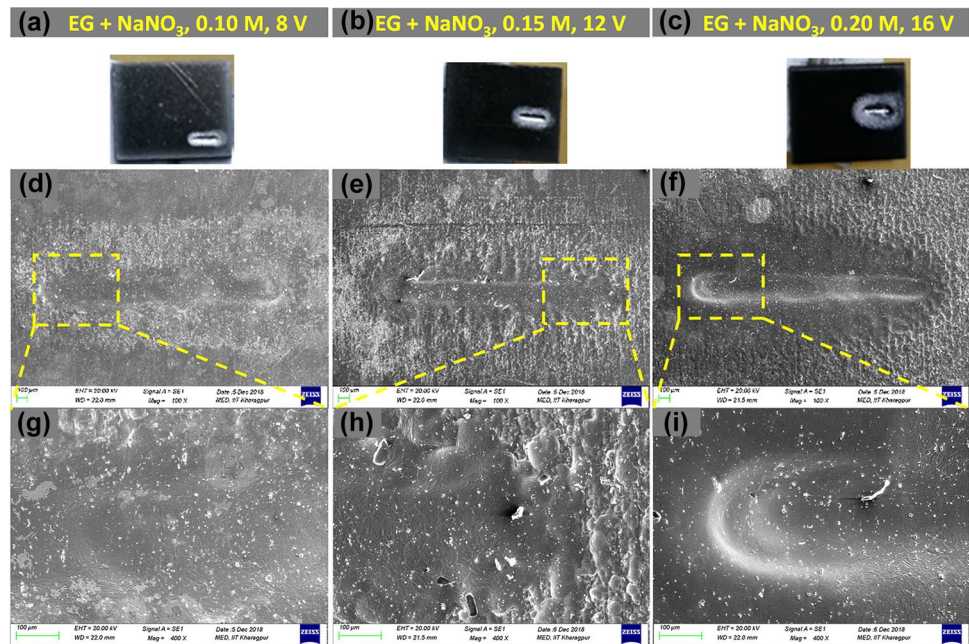
4.2 Effect of ethylene glycol-based NaNO₃ electrolyte on anodic dissolution of Nitinol

Among the three aqueous neutral electrolytes that were used for the generation of microchannel in Nitinol, only NaNO₃ was able to successfully machine Nitinol with better dissolution efficiency. However, the aqueous environment generates a large amount that hinders the further

dissolution of metal anode reducing the efficiency of dissolution. Also, in an aqueous electrolyte, the sludge gets deposited on the cathode surface which seriously affects the process quality and efficiency. The water-based electrolyte is known to form an oxide layer on the surface of titanium and its alloys which impairs the machining accuracy and produces a rough machining surface. Therefore, to overcome the above drawbacks, an alternative electrolyte was proposed for micro-ECM of Nitinol. The use of ethylene glycol instead of water can help to avoid the generation of oxygen on the anode and prevent the contact between oxygen and Nitinol. As water is a source of passivating oxygen, EG solutions are less effective passivator, and hence, a smooth surface will always be available for machining [37].

The experiments were repeated at three different levels with three different combinations of concentration and voltage for the EG + NaNO₃ electrolyte. Figure 12 shows the optical and SEM images of the fabricated microchannel in three different

Fig. 12 Machined specimen obtained in EG + NaNO₃ solutions through micro-ECM in three different parameters: **a–c** optical images, **d–f** SEM images, and **g–i** zoomed view of the microchannel



parameters for EG + NaNO₃ electrolyte. The EDS result of the machined surface is given in Table 5. From the optical images, it is observed that a bright surface was obtained at the machined region for all levels of parameters. The EDS data shows that no oxygen is present on the machined surface for all levels of parameters which implies that there is no passivation of the Nitinol surface in the EG + NaNO₃ electrolyte. Also, the average ratio of Ti and Ni is found to be around 43.5:55.5 for all the parameters which is nearer to the base material composition. This infers that there is a uniform dissolution of the machined surface in the case of the EG + NaNO₃ electrolyte. Figure 13 shows a relationship between average surface roughness (R_a) and the level of process parameters for aqueous NaNO₃ and EG + NaNO₃ electrolytes. The surface roughness of the machined surface obtained was 0.891 μm , 0.25 μm , and 0.424 μm for low-, mid-, and high-level parameters which is less in comparison to that obtained in the case of aqueous NaNO₃ solution. Thus, a smoother surface was obtained in the case of EG-based NaNO₃ electrolyte.

According to Liu et al. EG-based electrolytes exhibit a better machining performance due to their mass transfer-controlling dissolution, which is also known as the anode

Table 5 EDS data of sludge growth on the specimen for different electrolyte conditions under three levels of parameters

Electrolyte	Parameters	Element Weight (%)	
		Ti	Ni
EG + NaNO ₃	0.1 M, 8 V	43.50	56.50
	0.15 M, 12 V	43.49	56.51
	0.20 M, 16 V	44.10	55.90

polishing effect [37]. The polishing zone is formed on the anode surface which greatly improved the machined surface integrity and subsequently forms a bright surface as shown in Fig. 13. Also, other authors like Yusen et al. suggested that the dissolution process in EG solution is a mixed process of charge transfer and diffusion in comparison to only the charge transfer process in the aqueous solution [38]. In the case of EG-based electrolyte, the fluidity of the diffusion layer is low that slows the diffusion of ions, and hence, the rate of dissolution is relatively uniform

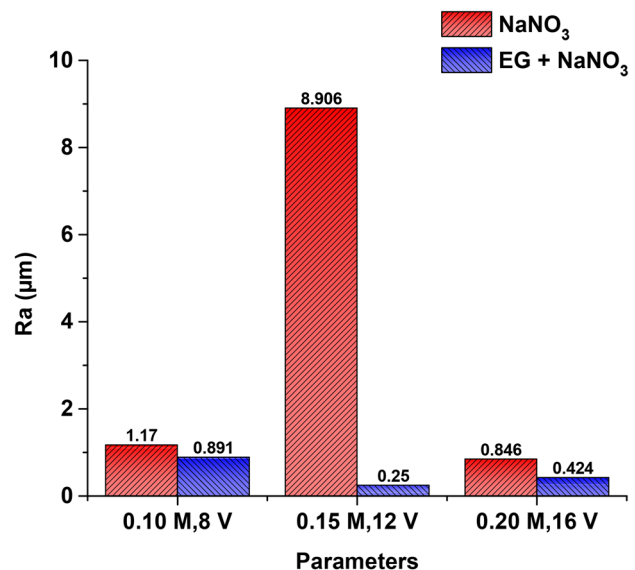


Fig. 13 Relationship between average surface roughness (R_a) and the level of process parameters for NaNO₃ and EG + NaNO₃ electrolytes

producing a smoother surface. Wang et al. found out that the diffusion layer that forms in the case of EG-based electrolytes is metal glycolates which are less conductive and viscous film that develops on the anode surface [39]. The liquid film that developed on the surface is colloidal in nature, and upon saturation, it tends to give faster dissolution at microprojections and slower at microrecess features, thus levels the surface for excellent surface integrity [40]. Both Ni and Ti components of Nitinol once anodically dissolved may form Ni and Ti glycolate complex directly with EG, stepwise according to the following equations.

In EG + NaNO₃ solution:



Thus, a uniform dissolution of Nitinol was obtained in the case of EG + NaNO₃ electrolyte. The use of EG-based electrolyte in lieu of aqueous electrolyte helps to avoid the generation of oxygen on the anode and prevents the contact between oxygen and Nitinol. As water is a source of passivating oxygen, EG solution is a much less effective passivator. Hence, the passive film is rarely generated after the smooth anode surface is exposed, and as Nitinol continues to dissolve, the machinability of Nitinol is better. Due to the polishing effect of EG + NaNO₃ on Nitinol, the lowest R_a value of 0.25 μm of the machined surface was obtained which is better than the surface roughness obtained by Ao et al. using EG + NaCl + ethanol electrolyte.

Figure 14 shows the variation of DOC, WOC, and LOC with respect to three levels of parameters for both aqueous NaNO₃ and ethylene glycol-based NaNO₃ electrolytes. From the figure, it can be observed that in comparison to aqueous solutions, ethylene glycol-based NaNO₃ produces lower DOC, WOC, and LOC. This is attributed to the low conductivity of ethylene glycol which produces low current density reducing the stray current effect thus minimizing the overcut. Also, the EG solution produces soluble complexes in ambient conditions and hence can be easily removed from the IEG [29]. These effects form a stable machining condition, and the conductivity of the electrolyte remains constant throughout the process, causing a reduction in overcut in depth, width, and length in comparison to aqueous solutions. However, from the SEM images in Fig. 12, it can be seen that the surface surrounding the microchannel in all three parameters is affected by bubble marks. These

bubble marks on the surface of Nitinol decrease the surface integrity of microfeatures. The bubbles are the hydrogen gas that is being generated at the cathode during the electrochemical reaction according to Eq. (22) [37]. During the dissolution process, these hydrogen gas bubbles do not affect the machining due to the rapid formation and explosion. However, when the IEG is too low, the machining process is continued with the proximity of bubbles to both the surface of the cathode and Nitinol. Due to the bubbles, the dissolution is uneven, and partial bubble marks are generated on the Nitinol surface [41]. Thus, for efficient machining, a suitable IEG is preferred. Also, proper insulation of the sidewall of the microtool is required to check the stray current that affects the accuracy of the fabricated microchannel. From the SEM images in Fig. 12, it is observed that with the increase in level, the bubble marks decrease. This is due to the increase in IEG as the concentration of the electrolyte increases.



4.3 Potentiodynamic polarization analysis of Nitinol

To understand the dissolution behavior of Nitinol, the PDP tests were performed in aqueous NaCl, aqueous NaNO₃, and aqueous NaBr solutions. The PDP test that is conducted here is cyclic voltammetry (CV). CV is one of the most popular methods for the quantitative analysis of an electrochemical reaction. CV gives data on redox reactions, adsorption processes, and heterogeneous electron transfer reactions [42]. This technique also locates the rapid changes of redox potentials of electroactive species in a solution. During the CV process, the potential of the stationary working electrode is scanned using a triangular waveform. The resulting current due to the electrochemical reaction at the electrode–electrolyte interface is then recorded by the potentiostat. The current response then plotted as a function of applied potential is called a cyclic voltammogram.

The first cyclic voltammogram of Nitinol in aqueous NaCl solution was recorded between 0 and 2 V (SCE) with 3 repetitive cycles at a scan rate of 20 mV/s at room temperature. The cyclic voltammogram of Nitinol in 0.1 M aqueous NaCl solution is given in Fig. 15a. It is apparent from the figure in cycle 1 that the current density increases rapidly as the potential increases from 0 V. However, at 0.8 V, the rate of increase in current density decreases. This may be due to the passivation of the working electrode as Nitinol forms an oxide layer composed of NiO and TiO₂ in the aqueous solution. At 1.6 V, the current density again starts to rise rapidly and linearly indicating the adsorption of Cl⁻ ion onto the passive oxide film which leads to the formation of soluble complex and

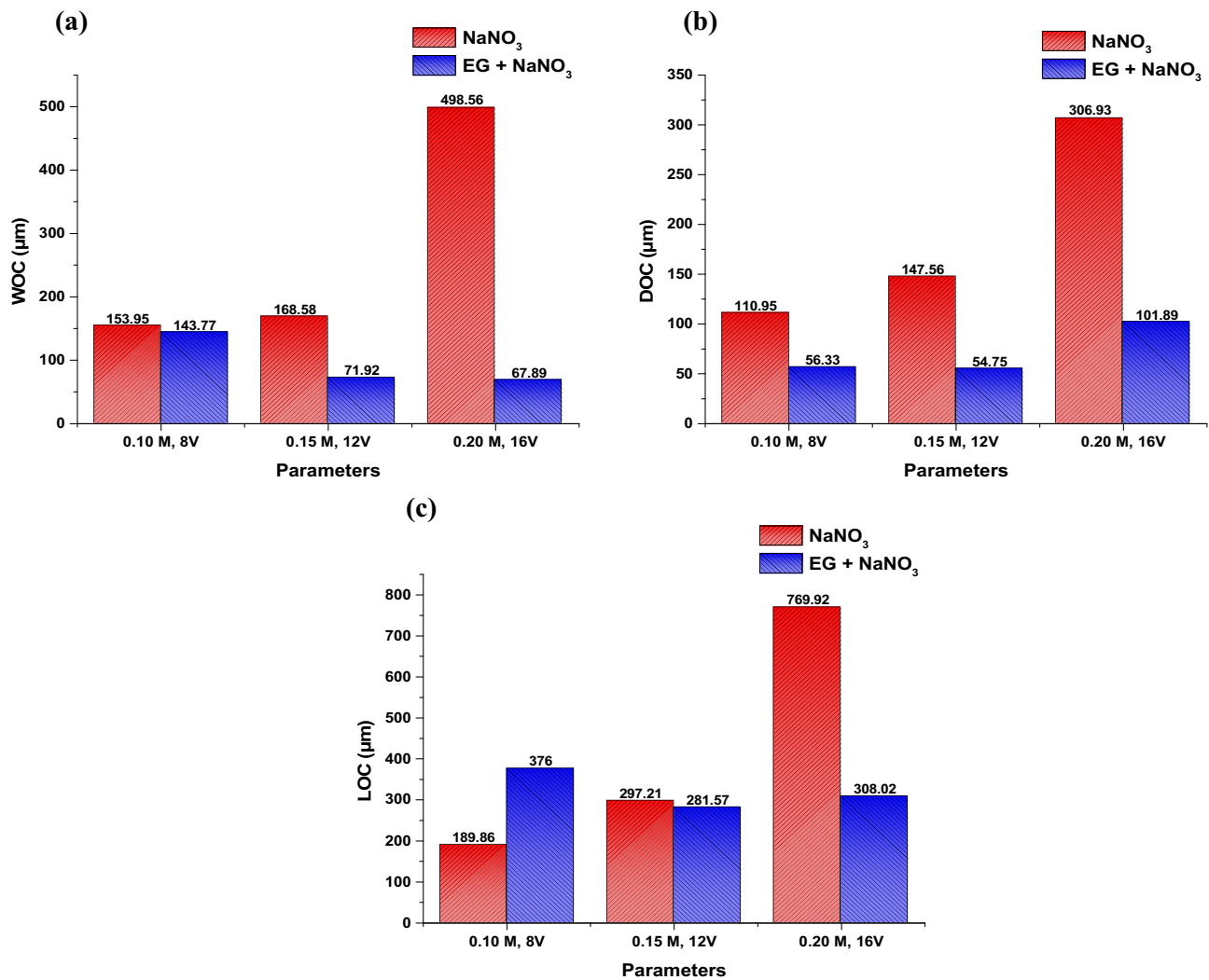
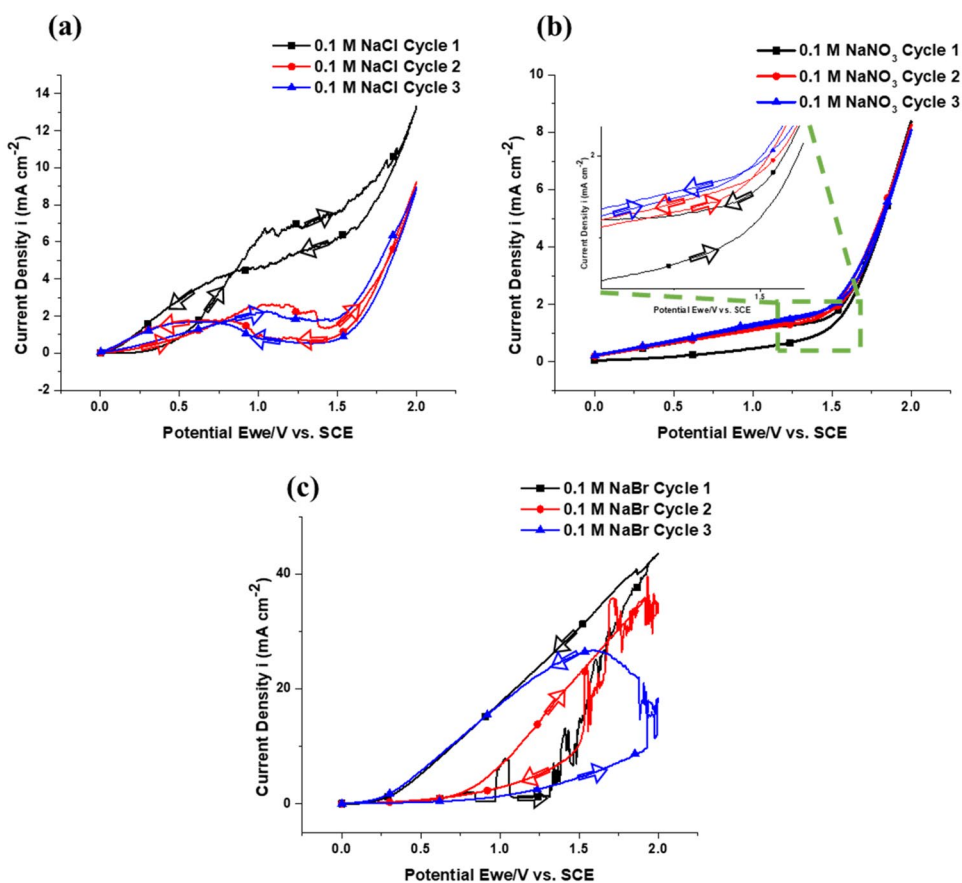


Fig. 14 Variation of **a** width overcut, **b** depth overcut, and **c** length overcut of the microchannels with respect to three levels of parameters machined through micro-ECM for electrolytes aqueous NaNO_3 and $\text{EG} + \text{NaNO}_3$

subsequent breakdown of the film with initialization and propagation of pitting. The maximum current density achieved is 13.33 mA cm^{-2} . In cycle 2, the current density decreases after 0.79 V indicating the passivation of Nitinol and again the current density linearly increases after 1.6 V breaking the passivation layer and a maximum current density was achieved is 9.25 mA cm^{-2} . It can be observed from the voltammogram that in subsequent cycling up to cycle 3, the maximum current density gradually decreases to 8.92 mA cm^{-2} . As discussed earlier, NiO in the oxide layer is more prone to dissolution compared to TiO_2 in the case of aqueous NaCl solution. The remaining TiO_2 , which is dense and sticky in nature, becomes more protective and stayed unreduced with successive cycling. Hence, it reduces the current and subsequent dissolution efficiency. Figure 15b shows the cyclic voltammogram of Nitinol in 0.1 M aqueous NaNO_3 solution measured

between 0 and 2 V. With the increase in the potential, the current density increases gradually up to 1.5 V. After 1.5 V, the current density increases very steeply up to 2 V. In the first cycle, the maximum current density achieved 8.39 mA cm^{-2} . However, with successive cycling, the maximum anodic current decreases from cycle 1 to cycle 3 up to 8.08 mA cm^{-2} . However, the rate of decrease of current density upon successive cycling is very less in the case of aqueous NaNO_3 in comparison to aqueous NaCl . This shows that upon successive cycling, the passive layer does not get protective, and subsequently, a uniform dissolution of both NiO and TiO_2 is achieved. Figure 15c shows the cyclic voltammogram of Nitinol in 0.1 M NaBr solution. From the figure, it can be seen that at a forward scan at 0.84 V, there is a sudden decrease in current density and it remains constant up to 0.96 V. This region can be attributed to the passivation region. Beyond this potential,

Fig. 15 Cyclic voltammogram of Nitinol in **a** 0.1 M NaCl solution, **b** 0.1 M NaNO₃ solution, and **c** 0.1 M NaBr solution



there is a rapid increase and sudden decrease in potential which can be attributed to the formation of micropits. From 1.06 to 1.31 V, the passivation of pits occurs and the current density remains constant; beyond 1.31 V, the

cyclic voltammogram becomes irregular with increasing current density. This region can be attributed to the propagation of pitting and high pitting occurrence. The maximum current density achieved at 2 V is 46.56 mA cm⁻²

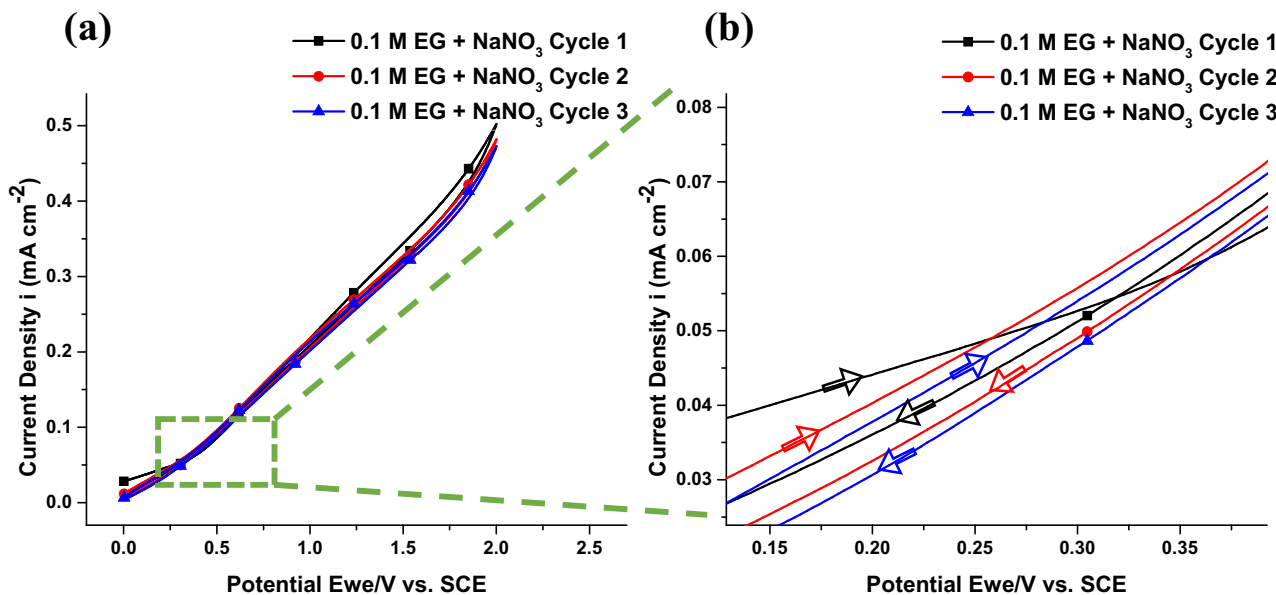


Fig. 16 Cyclic voltammogram of Nitinol in 0.1 M EG + NaNO₃ solution

which is much higher compared to both aqueous NaCl and NaNO₃ solutions. The Br⁻ ions form a soluble titanium complex on the surface thus exposing the NiO sublayer of the oxide film. As the resistance of pitting of NiO is much lower, it facilitates the frequent breakdown of the passive film resulting in a large number of pits on the surface. The cyclic voltammograms of Nitinol in EG + NaNO₃ are given in Fig. 16. It shows an active dissolution without any passivation, and the current density obtained for cycle 1 at 2 V is 0.502 mA cm⁻², which is very low in comparison to 8.39 mA cm⁻² for cycle 1 in aqueous NaNO₃. Also, upon successive cycling up to 3 cycles, the maximum current decreases to 0.472 mA cm⁻² suggesting negligible oxide formation on the surface. As there is no passivation, a smooth surface is always available and Nitinol continues to dissolve producing excellent surface integrity.

5 Conclusions

The present study successfully investigated the dissolution behavior of Nitinol in different aqueous and non-aqueous electrolytes for micro-ECM by means of machining microchannels in Nitinol. The aqueous electrolytes like NaCl, NaNO₃, and NaBr and non-aqueous electrolyte like EG + NaNO₃ were used for the study. Moreover, the potentiodynamic polarization analysis gives insight into the nature of the dissolution of Nitinol in both aqueous and non-aqueous electrolytes. The following conclusions were drawn from the experimental results.

- The average surface roughness of 0.848 μm of the machined microchannel in the case of NaNO₃ is found to be the lowest at the high level of parameters in comparison to that obtained with NaCl and NaBr electrolytes. In the case of NaNO₃ electrolyte, the oxide layer successfully dissolves into the electrolyte forming a soluble complex. Thus, a uniform dissolution is achieved. In the case of NaCl and NaBr, microchannel fabrication was not successful due to excessive passive layer formation that hinders the uniform dissolution of Nitinol.
- To overcome the passivation that arises due to the aqueous electrolyte, EG-based NaNO₃ was used to fabricate the microchannel. The electrolyte EG + NaNO₃ produces a polished bright surface with R_a value values 0.891 μm, 0.25 μm, and 0.424 μm for low, middle, and high levels of the parameters. As there is minimum or no passivation on the surface, Nitinol actively dissolves in the EG + NaNO₃ electrolyte to create a smooth surface.
- A more accurate microchannel was fabricated in EG + NaNO₃ electrolyte as lower WOC, DOC, and LOC were measured in comparison to aqueous NaNO₃. This is due to the low conductivity of the non-aqueous based

electrolyte which minimizes the stray current resulting in better accuracy.

- The cyclic voltammetry reveals that Nitinol shows passive dissolution in all three aqueous solutions. In the case of NaCl, the current density gradually decreases in the repetitive cycle as the oxide layer developed on the surface could not be dissolved hindering a uniform dissolution. In the case of NaNO₃, the reduction of current density in three repetitive cycles is very low confirming that the oxide layer gets dissolved subsequently in a uniform manner improving the dissolution efficiency of Nitinol. Nitinol in aqueous NaBr solution shows a higher current density in comparison to NaCl and NaBr, but rapid fluctuation in the voltammograms confirms the pitting of the surface in NaBr solution. Further, the voltammograms for EG + NaNO₃ solution show an active dissolution of Nitinol as there is no passivation of the machined surface thus producing a smoother surface in comparison to aqueous NaNO₃.

Author contribution All authors contributed to the study conception and design. Material preparation, data collection, and analysis were performed by Mr. Abhijeet Sethi, Mr. Biswesh Ranjan Acharaya, and Dr. Partha Saha. The first draft of the manuscript was written by Mr. Abhijeet Sethi, and all authors commented on previous versions of the manuscript. All authors read and approved the final manuscript.

Declarations

Conflict of interest The authors declare no competing interests.

References

1. Wang FE, Buehler WJ, Pickart SJ (1965) Crystal structure and a unique “martensitic” transition of TiNi. *J Appl Phys* 36:3232–3239. <https://doi.org/10.1063/1.1702955>
2. Kauffman GB, Mayo I (1997) The story of nitinol: the serendipitous discovery of the memory metal and its applications. *Chem Educ* 2:1–21. <https://doi.org/10.1007/s00897970111a>
3. Otsuka K, Ren X (2005) Physical metallurgy of Ti-Ni-based shape memory alloys. *Prog Mater Sci* 50:511–678. <https://doi.org/10.1016/j.pmatsci.2004.10.001>
4. Santoro M, Nicolay OF, Cangialosi TJ (2001) Pseudoelasticity and thermoelasticity of nickel-titanium alloys: a clinically oriented review. Part I: Temperature transitional ranges. *Am J Orthod Dentofac Orthop* 119:587–593. <https://doi.org/10.1067/mod.2001.112446>
5. Patel SK, Behera B, Swain B et al (2020) A review on NiTi alloys for biomedical applications and their biocompatibility. *Mater Today Proc* 33:5548–5551. <https://doi.org/10.1016/j.matpr.2020.03.538>
6. Kahn H, Huff MA, Heuer AH (1998) The TiNi shape-memory alloy and its applications for MEMS. *J Micromech Microeng* 8:213–221. <https://doi.org/10.1088/0960-1317/8/3/007>
7. Mahalik NP (2008) MEMS. Tata McGraw-Hill Publishing Company Limited, New Delhi

8. Fujita H (1998) Microactuators and micromachines Proc IEEE 86:1721–1732. <https://doi.org/10.1109/5.704278>
9. Fu Y, Du H, Huang W et al (2004) TiNi-based thin films in MEMS applications: a review. Sens Actuators A Phys 112:395–408. <https://doi.org/10.1016/j.sna.2004.02.019>
10. Mwangi JW, Nguyen LT, Bui VD et al (2019) Nitinol manufacturing and micromachining: a review of processes and their suitability in processing medical-grade nitinol. J Manuf Process 38:355–369. <https://doi.org/10.1016/j.jmapro.2019.01.003>
11. Kowalczyk M (2017) Application of Taguchi method to optimization of surface roughness during precise turning of NiTi shape memory alloy. Photonics Appl Astron Commun Ind High Energy Phys Exp 2017(10445):104455G. <https://doi.org/10.1117/12.2281062>
12. Kuppuswamy R, Yui A (2017) High-speed micromachining characteristics for the NiTi shape memory alloys. Int J Adv Manuf Technol 93:11–21. <https://doi.org/10.1007/s00170-015-7598-9>
13. Wells SL (2013) Microdrilling of nitinol. Texas A&M University
14. Huang H, Zhang H, Zhou L, Zheng HY (2003) Ultrasonic vibration assisted electro-discharge machining of microholes in Nitinol. J Micromech Microeng 13:693–700. <https://doi.org/10.1088/0960-1317/13/5/322>
15. Unune DR, Nirala CK, Mali HS (2019) Accuracy and quality of micro-holes in vibration assisted micro-electro-discharge drilling of Inconel 718. Meas J Int Meas Confed 135:424–437. <https://doi.org/10.1016/j.measurement.2018.11.067>
16. James S, Mahajan A (2018) Experimental study of machining of smart materials using submerged abrasive waterjet micromachining process. ASME Int Manuf Sci Eng Conf MSEC 4:1–8. <https://doi.org/10.1115/MSEC2018-6494>
17. Katona B, Bognár E, Berta B et al (2013) Chemical etching of nitinol stents. Acta Bioeng Biomech 15:3–8. <https://doi.org/10.5277/abb130401>
18. Lee ES, Shin TH, Kim BK et al (2007) Electrochemical micromachining of nitinol by confined-etchant-layer technique. Int J Mach Tools Manuf 127:28–56. <https://doi.org/10.1016/j.ijmachtools.2018.01.004>
19. Lee ES, Shin TH, Kim BK, Baek SY (2010) Investigation of short pulse electrochemical machining for groove process on Ni-Ti shape memory alloy. Int J Precis Eng Manuf 11:113–118. <https://doi.org/10.1007/s12541-010-0014-3>
20. Saxena KK, Qian J, Reynaerts D (2018) A review on process capabilities of electrochemical micromachining and its hybrid variants. Int J Mach Tools Manuf 127:28–56. <https://doi.org/10.1016/j.ijmachtools.2018.01.004>
21. Mingcheng G, Yongbin Z, Lingchao M (2019) Electrochemical micromachining of square holes in stainless steel in H₂SO₄. Int J Electrochem Sci 14:414–426. <https://doi.org/10.20964/2019.01.40>
22. Anasane SS, Bhattacharyya B (2016) Experimental investigation on suitability of electrolytes for electrochemical micromachining of titanium. Int J Adv Manuf Technol 86:2147–2160. <https://doi.org/10.1007/s00170-015-8309-2>
23. Pooranachandran K, Deepak J, Hariharan P, Mouliprasanth B (2019) Effect of flushing on electrochemical micromachining of copper and Inconel 718 alloy. In: Vijay Sekar KS, Gupta M, Arockiarajan A (eds) Advances in Manufacturing Processes. Springer Singapore, Singapore, pp 61–69
24. Sethi A, Acharya BR, Saha P (2019) Fabrication of high aspect ratio cylindrical tungsten micro tool by reverse micro-ECM process. Int J Precis Technol 8:201. <https://doi.org/10.1504/ijptech.2019.10022607>
25. Sethi A, Acharya BR, Saha P (2022) Electrochemical dissolution of WC-Co micro-tool in Micro-WECM using an ecofriendly citric acid mixed NaNO₃ electrolyte. J Electrochem Soc 169:033503. <https://doi.org/10.1149/1945-7111/ac54d9>
26. Mineta T (2004) Electrochemical etching of a shape memory alloy using new electrolyte solutions. J Micromech Microeng 14:76–80. <https://doi.org/10.1088/0960-1317/14/1/310>
27. Ma XZ, Zhang L, Cao GH et al (2007) Electrochemical micromachining of nitinol by confined-etchant-layer technique. Electrochim Acta 52:4191–4196. <https://doi.org/10.1016/j.electacta.2006.11.046>
28. Maurer JJ, Hudson JL, Fick SE et al (2012) Electrochemical micromachining of NiTi shape memory alloys with ultrashort voltage pulses. Electrochem Solid-State Lett 15:28–30. <https://doi.org/10.1149/2.002202esl>
29. Ao S, Li K, Liu W et al (2020) Electrochemical micromachining of NiTi shape memory alloy with ethylene glycol–NaCl electrolyte containing ethanol. J Manuf Process 53:223–228. <https://doi.org/10.1016/j.jmapro.2020.02.019>
30. Mouliprasanth B, Hariharan P (2021) Influence of variant electrolyte in electrochemical micromachining of micro holes in SMA using Taguchi optimization. Russ J Electrochem 57:197–213. <https://doi.org/10.1134/S1023193521030095>
31. Ding R, Shang JX, Wang FH, Chen Y (2018) Electrochemical Pourbaix diagrams of Ni–Ti alloys from first-principles calculations and experimental aqueous states. Comput Mater Sci 143:431–438. <https://doi.org/10.1016/j.commatsci.2017.11.033>
32. Asserghine A, Medvidović-Kosanović M, Nagy L, Nagy G (2019) In situ monitoring of the transpassivation and repassivation of the passive film on nitinol biomaterial by scanning electrochemical microscopy. Electrochem Commun 107:106539. <https://doi.org/10.1016/j.elecom.2019.106539>
33. Wang Y, Wei X, Li Z et al (2020) Electrolytic polishing of nitinol based cardiovascular stent in NaCl-ethylene glycol-ethanol-water electrolyte. Int J Electrochem Sci 15:8823–8836. <https://doi.org/10.20964/2020.09.01>
34. Davydov AD, Kabanova TB, Volgin VM (2017) Electrochemical machining of titanium. Review Russ J Electrochem 53:941–965. <https://doi.org/10.1134/S102319351709004X>
35. Zarubitskii OG, Dmitruk BF, Zakharchenko NF (2007) Titanium interaction with hydroxide-salt melts. Prot Met 43:483–486. <https://doi.org/10.1134/S0033173207050116>
36. Muñoz-Portero MJ, García-Antón J, Guiñón JL, Pérez-Herranz JL (2007) Pourbaix diagrams for nickel in concentrated aqueous lithium bromide solutions at 25 °C. Corrosion 63:625–634. <https://doi.org/10.5006/1.3278412>
37. Liu W, Zhang H, Luo Z et al (2018) Electrochemical micromachining on titanium using the NaCl-containing ethylene glycol electrolyte. J Mater Process Technol 255:784–794. <https://doi.org/10.1016/j.jmatprotec.2018.01.009>
38. Yusen H, Tao Y, Zhengyang X, Yongbin Z (2021) Electrochemical micromachining of ZrCu-based amorphous alloy in ethylene glycol solution. Intermetallics 132:107155. <https://doi.org/10.1016/j.intermet.2021.107155>
39. Wang J, Torres-Sanchez C, Borgman JM et al (2020) Template-free, microscale dimple patterning of pure titanium surface through anodic dissolution using non-aqueous ethylene glycol-TiCl₄ electrolytes. Surf Coatings Technol 404:126555. <https://doi.org/10.1016/j.surfcoat.2020.126555>
40. Hryniewicz T (1994) Concept of microsmoothing in the electropolishing process. Surf Coatings Technol 64:75–80. [https://doi.org/10.1016/S0257-8972\(09\)90006-8](https://doi.org/10.1016/S0257-8972(09)90006-8)
41. Lee ES, Shin TH (2011) An evaluation of the machinability of nitinol shape memory alloy by electrochemical polishing. J Mech Sci Technol 25:963–969. <https://doi.org/10.1007/s12206-011-0209-2>
42. Elgrishi N, Rountree KJ, McCarthy BD et al (2018) A practical beginner's guide to cyclic voltammetry. J Chem Educ 95:197–206. <https://doi.org/10.1021/acs.jchemed.7b00361>

Publisher's note Springer Nature remains neutral with regard to jurisdictional claims in published maps and institutional affiliations.